https://doi.org/10.5194/egusphere-2025-4569
Preprint. Discussion started: 15 January 2026

Dynamic and Thermal Analysis of Sandstorm Processes Based on Vertical Observation Data

Yifei Wang[1,2,3,4,5], Wen Huo[1,3,4,5], Yongqiang Liu[1,2,3,4,5], Mayibaier Maihamuti[1,2,3,4,5], Fan Yang[1,3,4,5], Chenglong Zhou[1,3,4,5], Xinghua Yang[1,3,4,5,6], Ali Mamtimin[1,3,4,5]

1.Institute of Desert Meteorology, China Meteorological Administration, Urumqi 830002, China
2.College of Geography and Remote Sensing Sciences, Xinjiang University, Urumqi 830046, China
3.National Observation and Research Station of Desert Meteorology, Taklimakan Desert of Xinjiang, Urumqi 830002, China
4.Taklimakan Desert Meteorology Field Experiment Station, China Meteorological Administration, Urumqi 830002, China
5.Xinjiang Key Laboratory of Desert Meteorology and Sandstorm, Urumqi 830002, China
6.School of Geographical Sciences, Shanxi Normal University, Taiyuan 030032, China

Corresponding Author: Wen Huo huowenpet@idm.cn orcid:0000-0002-7861-2424

Abstract: The Taklamakan Desert (TD) is a key source of dust storms in East Asia, frequently impacting China and neighboring countries. Based on dual-gradient observational experiments in the central and peripheral regions of the TD, combined with ERA5 data and HYSPLIT analysis, eight dust storms from April to June 2024 were studied. The findings include:(1)Dust storm trajectories in the TD fall into three types: (a) east-to-west movement, (b) transport across the Tianshan and Pamir Mountains, and (c) west-to-east movement driven by thermal factors in summer.(2)Spring dust storms (March–April) are dominated by dynamic factors, while summer storms (May–June) are influenced by thermal factors. Significant pressure and temperature changes 12–6 hours before a storm provide a critical prediction window.(3)Horizontal dust flux (Q) at XiaoTang (peripheral region) follows a parabolic pattern, while at TaZhong (central region), terrain plays a key role. High Q values result in larger fluctuations, while low Q values show relative stability. Seasonal temperature differences, convective intensity, and flat terrain drive alternating wind speed trends at XiaoTang before storms, with stronger fluctuations observed in summer due to rising temperatures.

Keywords: Dust Storms, Backward Trajectory Analysis, Causation Analysis, Horizontal And Vertical Dust Flux Analysis

1 Introduction

Dust storms are one of East Asia's most severe natural disasters, occurring frequently in arid and semi-arid regions such as the Taklamakan Desert in China and the Gobi Desert bordering Mongolia. These events are widespread in spring, impacting millions(Bao & Fang, 2007; Shao & Dong, 2006). Dust storms are often accompanied by air pollution, strong winds, and significant reductions in visibility, severely affecting human life and production activities. These disasters disrupt agriculture, transportation, and infrastructure and pose threats to public health, particularly by significantly increasing the incidence of respiratory diseases(Achakulwisut et al., 2018; Manisalidis et al., 2020; Mohebbi et al., 2019; Tong et al., 2023; Wen et al., 2024).In addition, dust storms negatively impact ecosystems by causing soil degradation and water source

https://doi.org/10.5194/egusphere-2025-4569
Preprint. Discussion started: 15 January 2026

contamination, further exacerbating the ecological vulnerability of affected regions (Ma et al., 2020; Perez et al., 2008).

Meanwhile, the frequent occurrence of dust storms may also intensify global climate change and exacerbate challenges in cross-regional environmental governance(Prospero, 1999; Zong et al., 2021). The Taklamakan Desert is in Asia's arid and semi-arid regions, characterized by scarce precipitation, vast sandy terrain, and dry climatic conditions. Combined with the influence of Mongolian cyclones, these factors make the region prone to frequent dust storms in spring, establishing it as one of the primary dust sources in East Asia (Shao & Dong, 2006; Xu et al., 2020).

The formation of dust storms is a complex physical process driven by interactions between the atmosphere and surface soil, where dust source materials, dynamic conditions, and thermal factors play critical roles in influencing their occurrence. The characteristics and quantity of dust source materials determine the generation and intensity of dust. As the dynamic condition, wind is the primary direct factor triggering dust storms, while thermal factors provide strong supportive conditions for their occurrence(Iversen & White, 1982). The formation of dust storms is also influenced by various factors related to surface dust source materials, including dust particle size, soil moisture, and vegetation cover. When soil particle size exceeds 60–70 μm, the threshold for dust emission increases gradually with particle size due to the gravitational influence of the particles themselves. Conversely, when particle size is less than 60–70 μm, the increased cohesive forces between particles significantly raise the dust emission threshold as particle size decreases (Iversen & White, 1982; Marticorena & Bergametti, 1995).In addition, soil particle size affects dust emission flux during dust storm events(Yang et al., 2016). Soil moisture is likewise a crucial influencing factor. On one hand, higher moisture levels enhance the adhesive forces between particles; conversely, they promote the aggregation of fine particles, thereby suppressing sand mobilization and reducing dust fluxes(Iversen & White, 1982; Shao & Dong, 2006). The increase in vegetation effectively suppresses the occurrence of dust storms or mitigates their intensity by reducing the supply of sand sources and dissipating wind energy(MacKinnon et al., 2004; Raupach, 1992).

In East Asia during spring, there is a significant positive correlation between strong winds and the frequency of dust storms (Xu et al., 2020).In East Asia, Mongolian cyclones frequently generate strong winds, which in turn lead to the formation of dust storms. These cyclones exhibit pronounced seasonality (March to May) and are typically accompanied by weather conditions such as strong winds, temperature drops, dust emissions, and significant reductions in visibility.Their impact is not confined to Mongolia and northern China but can extend across the entire East Asian region. Through upper-atmosphere circulation, these effects may even spread to more distant areas, such as Korea, Japan, and the western Pacific coast(Liu et al., 2004; X. Wang et al., 2009)

Horizontal and vertical dust fluxes jointly determine the spatial extent of dust dispersion, which is critical in shaping global dust transport pathways. High vertical dust fluxes can transport dust to more distant regions, thereby influencing atmospheric chemical composition, climate systems, and ecological environments. Accurately understanding dust flux is crucial for improving dust storm forecasting, particularly within climate models, as it aids in better predicting the impacts of dust on air quality and ecosystems(S. Chen et al., 2023b). Recent studies have focused on this field, revealing several significant findings. Research by (Kai & Huiwang, 2007) identified

https://doi.org/10.5194/egusphere-2025-4569
Preprint. Discussion started: 15 January 2026

three primary transport pathways for East Asian dust storms:1) Passing through China and depositing in the Bohai Sea, Korea Strait, Sea of Japan, and Yellow Sea;2) Extending westward into Central Asia;3) Reaching as far as the western Pacific under the influence of strong northwesterly winds. Additionally, many researchers have utilized the WRF-Chem model to analyze dust emissions from different regions, thereby improving the numerical prediction of dust storms, particularly in terms of transport and deposition calculations(DeMeester & Johnson, 1975; Hosseini Dehshiri & Firoozabadi, 2024; Rizza et al., 2017; Y. Zeng et al., 2020). For the Taklamakan Desert, observational data from (Aili et al., 2023)indicate a significant decreasing trend in deposition rates across different underlying surfaces in the northeastern desert-oasis transitional zone. The order is as follows: mobile sand desert > semi-mobile sand desert > desert vegetation > shelterbelt forest > farmland. This demonstrates the effectiveness of increased vegetation in suppressing dust storms. Improved WRF-Chem simulation results by (Y. Chen et al., 2023) indicate that in the Taklamakan Desert, the formation of summer dust storms is primarily influenced by thermal factors. In contrast, spring dust storms are dominated by dynamic factors.(Huo et al., 2022), based on dual-gradient observational experiments in the central and peripheral regions of the desert, found that in flat areas, horizontal dust flux (Q) and vertical dust flux (F) exhibit a linear relationship and an exponential variation with height. However, no significant changes were observed over undulating terrain.(H. Wang et al., 2015), through field observations, measured the horizontal wind erosion flux and dust emissions during windblown sand/dust processes across arid and semi-arid regions in northern China. Their findings revealed that the Taklamakan Desert exhibits significantly stronger horizontal dust flux than other studied regions, thus identifying it as a significant source of dust emissions.

In summary, due to observational methods' limitations, most studies rely on remote sensing data to calculate horizontal and vertical dust fluxes (Q and F) or analyze observational data. Few studies have successfully integrated both approaches. Research that integrates multiple data sources to comprehensively analyze the variations in Q and F and the underlying driving factors is relatively scarce and remains an area for further exploration. In this context, the present study conducted dual-point gradient synchronous dust storm observational experiments in the Taklamakan Desert, obtaining multiple key parameters and their differences under various topographical conditions. It also incorporated reanalysis data and backward trajectory analysis. This approach further enhanced the ability to analyze the dynamic characteristics of dust storms. Remote sensing data strongly supports the spatial distribution and diffusion of dust storms on a large scale. At the same time, backward trajectory analysis effectively traces dust storms' origins and transport pathways. Combining multiple data sources, this approach overcomes the limitations of single observational methods and offers a more comprehensive analytical perspective.

Through the comprehensive analysis of these data, the study provides an in-depth understanding of how different topographical features in the Taklamakan Desert influence key parameters of dust storms. It also offers strong technical support for investigating, monitoring, and predicting dust storm formation. This deepens the understanding of dust storm characteristics and their evolution and enhances the recognition of the Taklamakan Desert's influence on dust emissions and transport in Asia and globally. This provides valuable reference points for future related research and lays a solid scientific foundation for preventing and managing dust storms.

Section 2 of this paper describes the study area, the data used, and the methodology. Section 3 analyzes dust trajectories, the meteorological background of dust storms, and their dynamic and

https://doi.org/10.5194/egusphere-2025-4569
Preprint. Discussion started: 15 January 2026

thermal factors. It also examines the horizontal and vertical fluxes and temperature and wind speed variations across different desert topographies based on observational data. The discussion and conclusions are presented in Sections 4 and 5, respectively.

2 Study Area, Data, and Methodology

2.1 Study Area

The Taklamakan Desert (TD) is located within the Tarim Basin in the southwestern part of the Xinjiang Uyghur Autonomous Region in China. It is the second-largest shifting sand desert in the world. Surrounded by mountain ranges such as the Tianshan and Kunlun Mountains, the region experiences a highly arid climate. Key characteristics of the desert include its remoteness from the ocean, sparse vegetation, diverse dune types with high mobility, extensive and thick shifting sand areas, and fine sand particles. This region is subject to frequent dust storms year-round and is one of the significant sources of dust storms in East Asia(Sun & Liu, 2006).

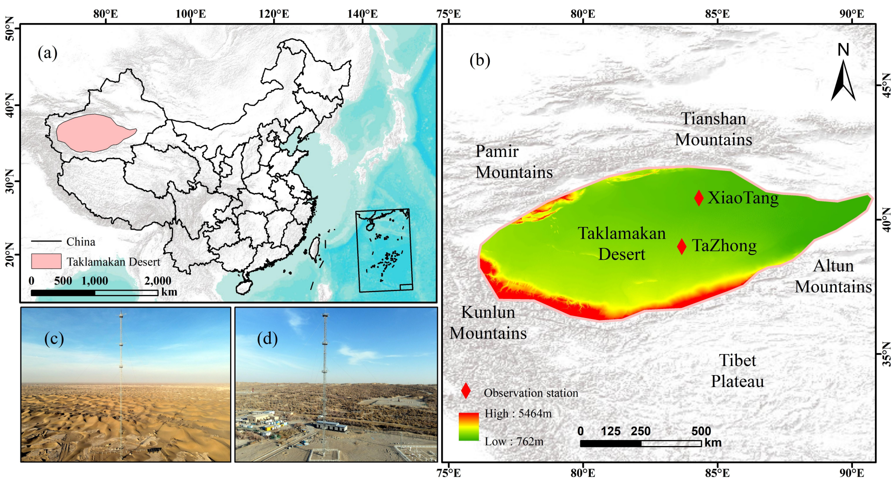

Fig. 1 Location and topography of the Taklimakan Desert, and the TZ and XT observation towers (maps and site photos)

2.2 Observational Data

The observational data were obtained from two stations: X Station, located on the northern edge of the Taklamakan Desert, representing flat terrain, and TZ Station, situated in the desert interior, representing undulating terrain. TZ Station is at an elevation of 80 meters, while X Station is at 100 meters. Both stations are equipped with gradient observation systems and collection systems. The gradient layers at TZ Station are at 1 m, 2 m, 5 m, 8 m, 16 m, 24 m, 32 m, 47 m, 63 m, and 80 m. At XT Station, they are at 1 m, 2 m, 5 m, 10 m, 24 m, 32 m, 47 m, 63 m, 80 m, and 100 m.

The gradient observation system records climate parameters at each layer, including hourly and minute-based measurements of temperature, humidity, wind speed, wind direction, and atmospheric pressure. The gradient collection system gathers dust samples during dust storms using BSNE (Big Spring Number Eight) dust collectors installed at each layer, which are used to determine the horizontal dust flux at different heights.

https://doi.org/10.5194/egusphere-2025-4569
Preprint. Discussion started: 15 January 2026

Nine dust storm events were observed between April 3 and July 10, 2024 (as detailed in Table 1). However, during the second observation, data from the TZ Station were missing, preventing a complete record. Therefore, the remaining eight observations became the primary samples for this study.

Tab. 1 Sample details

	Station Name	Start time of dust storm	Duration time(h)	Sample collection time
1	TZ	2024.3.31	22	2024.4.3
	XT	2024.3.31	17.3	2024.4.4
2	XT	2024.4.5	5	2024.4.6
3	TZ	2024.4.12	24	2024.4.16
	XT(	2024.4.12	7.5	2024.4.15
4	TZ	2024.4.17	36	2024.4.20
	XT	2024.4.17	23	2024.4.21
5	TZ	2024.4.26	17.5	2024.5.12
	XT	2024.4.26	42.5	2024.5.12
6	TZ	2024.5.12	24	2024.5.16
	XT	2024.5.12	55	2024.5.17
7	TZ	2024.5.20	40	2024.6.3
	XT	2024.5.20	27.5	2024.5.30
8	TZ	2024.6.4	12	2024.6.10
	XT	2024.6.4	7	2024.6.10
9	TZ	2024.6.18	58	2024.7.9
	XT)	2024.6.18	22	2024.7.10

2.3 Remote Sensing Data

To further investigate the causes of dust storms, the study analyzed relevant meteorological conditions using the ERA5 reanalysis dataset. ERA5, provided by the European Centre for Medium-Range Weather Forecasts (ECMWF), is the fifth generation of global climate and weather reanalysis data. It has a spatial resolution of 0.25° × 0.25° and a temporal resolution of 1 hour.

The ERA5 reanalysis dataset has demonstrated high accuracy in East Asia and desert regions. (Y. Wang et al., 2023)compared observational meteorological parameters from the Gurbantünggüt Desert with ERA5, MERRA2, JRA-55, and NCEP-FNL data and found that ERA5 had the most minor error. To assess their reliability and accuracy, (Y. Wang et al., 2023)compared reanalysis data from NCEP/NCAR, NCEP/DOE, NCEP/CFSR, JRA-25, ERA-Interim, and MERRA (with observational data. The results showed that the mean values of geopotential height and temperature from these reanalysis datasets were generally consistent with the observational data. However, regarding specific humidity, the performance of NCEP/NCAR, NCEP/DOE, and NCEP/CFSR was inferior to that of the JRA-25, ERA-Interim, and MERRA products.

2.4 HYSPIT model

The study used the Hybrid Single-Particle Lagrangian Integrated Trajectory (HYSPLIT) model to analyze the transport pathways of each dust storm event. This model utilizes grid data from the Global Data Assimilation System (GDAS) dataset to compute backward trajectories (Stein et al., 2015). The method assumes that the trajectory of a particle moving within the wind

https://doi.org/10.5194/egusphere-2025-4569
Preprint. Discussion started: 15 January 2026

field is the integral of the particle's changes over time and space, with its vector velocity determined by linear interpolation in both space and time. The final position of the air mass is calculated using the following equation:

$$P_1(t+\Delta t) = P(t) + V(P,t)\Delta t$$
$$P(t+\Delta t) = P(t) + 0.5[V(P,t) + V(P_1, t+\Delta t)]\Delta t$$

In this equation, P represents the initial position, P_1 is the first guessed position, Δt is the time interval, and V is the velocity of the air mass or particle. The simulation can be conducted online at the following link: https://www.ready.noaa.gov/HYSPLIT_traj.php.

2.5 The calculation of horizontal dust flux (Q) and vertical dust flux (F)

There are two primary methods for obtaining Q: the first is direct measurement in the field using various dust collection instruments; the second involves wind tunnel simulation experiments, where empirical equations are established between Q and wind speed u or friction velocity u^*, and Q is then inferred based on observed u or u^* values. In this experiment, direct measurement was employed. Professional personnel were hired to check the BSNE dust collectors daily to ensure they were clean and dust-free. After each dust storm, dust samples were collected and weighed on-site.

Both domestic and international dust mobilization experiments commonly use the two-layer dust concentration gradient method to calculate F(Gillette & Passi, 1988; X. Zeng & Dickinson, 1998; Zhang et al., 2017). The formula is as follows:

$$F = ku_*\frac{(c_1 - c_2)}{ln\,(z_2/z_1)}$$

In the formula, F represents the vertical dust flux (kg/m²/s); z_1 and z_2 are the measurement heights (m); u^* is the friction velocity (cm/s); c_1 and c_2 are the dust concentrations at the two heights (kg/m³); and k is a constant (0.4). The dust concentration ccc can be obtained by converting the dust transport data measured by the dust collectors:

$$c = \frac{M}{utA}$$

In the formula, c represents the dust concentration at the measurement height (kg/m³/s); M is the dust mass collected by the BSNE dust collector at the measurement height (kg); u is the average wind speed during the sampling period at the measurement height (m/s); t is the sampling time (s); and A is the inlet area of the BSNE dust collector (m²).

The formula for calculating friction velocity is as follows:

$$u(z) = \frac{u_*}{k} ln\,\frac{z}{z_o}$$

In the formula, u represents the wind speed at the observation height (cm/s); u^* is the friction velocity (cm/s); z is the observation height (cm); z_0 is the surface roughness length (cm); and k is a constant (0.4).

3 Results and Analysis

3.1 Dust Storm Trajectory Analysis

https://doi.org/10.5194/egusphere-2025-4569
Preprint. Discussion started: 15 January 2026

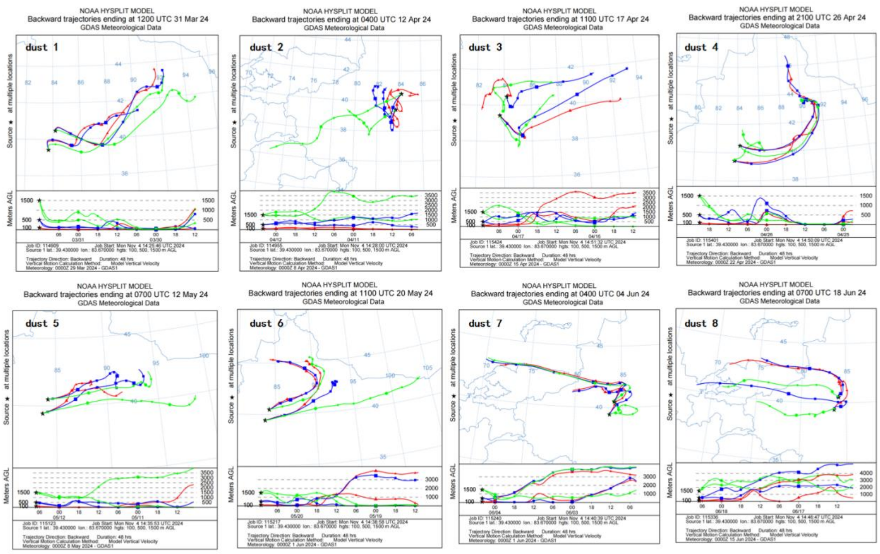

Fig. 2 Schematic diagram of the backward trajectory of these dust storms

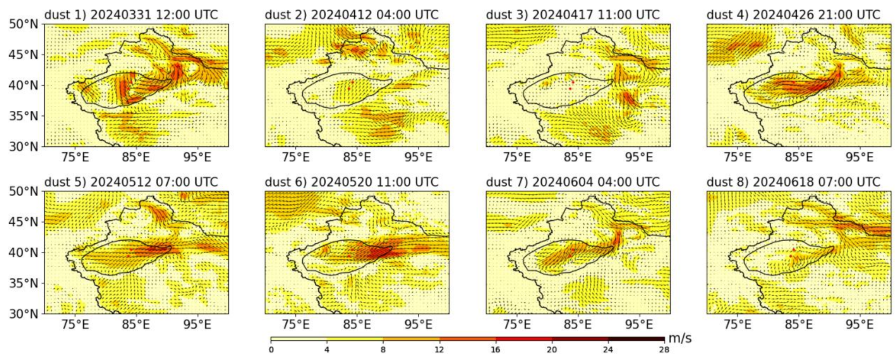

Fig. 3 10m wind vector plume field diagram

As shown in Figure 2, the eight dust storm events are labeled Dust1 through Dust8, and backward trajectory simulations were conducted using the HYSPLIT model. The results show that the dust trajectories can be classified into three types: Dust1, Dust3, Dust4, Dust5, and Dust6 move from east to west, passing through a gap in the northeastern Tarim Basin before entering the desert; Dust2 originates from the Indian subcontinent, crossing the Tibetan Plateau to enter the desert; Dust7 and Dust8 are from airflow originating in southern Russia and eastern Uzbekistan, and after long-distance transport, they cross the Tianshan Mountains before reaching the desert.

The TD covers the surface with loose materials such as gravel, and strong winds carry large dust particles. The anomalous variation in wind speed is closely related to the occurrence of dust storms. Therefore, wind speed anomaly trajectories can reflect the transport paths of dust storms. Using the 10m wind components u and v from ERA5's "single-level hourly data since 1940," wind field maps were generated (Fig. 3). The figure shows that for Dust1, Dust4, Dust5, Dust6, Dust7, and Dust8, strong winds primarily enter the desert through a gap on the eastern side of the Tarim Basin, with Dust1, Dust4, Dust5, and Dust6 experiencing powerful winds. Some strong winds in

https://doi.org/10.5194/egusphere-2025-4569
Preprint. Discussion started: 15 January 2026

Dust1, Dust3, Dust4, Dust6, Dust7, and Dust8 exhibit a north-to-south trend, crossing the Tianshan Mountains. In contrast, the strong winds, Dust2, blow from south to north from Tibet towards southern Xinjiang, consistent with the results from the backward trajectory model.

In summary, the backward trajectory analysis conducted using the HYSPLIT model based on the observation station coordinates effectively reveals the dust source trajectories passing through the stations before the occurrence of dust storms. However, it cannot fully reflect the direction of wind and its sources across the desert region. In contrast, ERA5 reanalysis data reveal the anomalous wind speeds corresponding to the HYSPLIT model and provide wind speed information for the Tarim Basin region, offering more comprehensive data for dust trajectory analysis. Based on the combined analysis of both datasets, the conclusion can be drawn that the dust storm trajectories in the TD are complex, with no single directional input, but rather a composite result of multiple directions. Most dust trajectories move from east to west, entering the desert through a gap on the eastern side of the Tarim Basin. The subsequent most common trajectories involve dust moving from north to south over the Tianshan Mountains. In contrast, fewer trajectories are observed moving from south to north across the Tibetan Plateau and over the Kunlun Mountains.

3.2 Dust Storm Dynamic and Thermal Meteorological Background

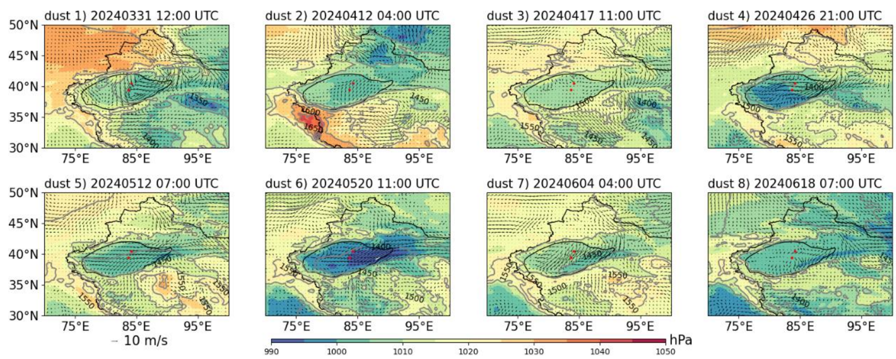

Fig.4 Mean sea level pressure, 10m wind vector, 850Phm altitude field

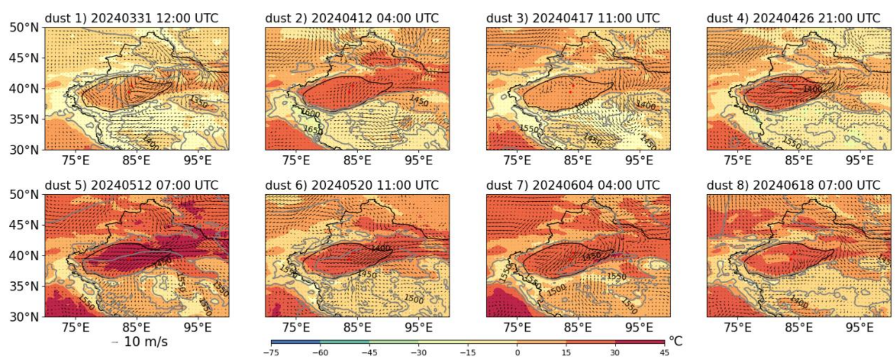

Fig.5 2m temperature, 10m wind vector, 850Phm altitude field

Figure 4 shows the average sea-level pressure (hPa), 850 hPa geopotential height (m), and 10 m horizontal wind (m·s^{-1}) for the periods leading up to Dust1-8. In all eight events, the north, west, and southwest regions of the Taklamakan Desert (TD) exhibited higher-than-average sea-level pressure and geopotential height than the TD area. In the cases of Dust1, Dust3, Dust4, Dust5, and Dust6, there was a significant pressure difference between eastern Kazakhstan, southern Russia, northern Xinjiang, and the Taklamakan Desert (TD) region. This pressure gradient caused most airflow trajectories to enter the TD through the gap in the eastern Tianshan Mountains. However, some airflows crossed the western and central Tianshan Mountains before reaching the desert. For Dust2, the average sea-level pressure in the southwestern region, near the northern border of Pakistan and northern India, was 1050 hPa, with a geopotential height of 1065 m. In contrast, the pressure in the Tarim Basin region was between 1000 and 1010 hPa, with a geopotential height of 1450 m. This climatic background led to strong upper-level winds crossing the Pamir and Kunlun Mountains, ultimately entering the Taklamakan Desert (TD). In the cases of Dust7 and Dust8, the pressure gradient in the TD region was not as significant as in the surrounding areas, and it was not easy to indicate the direction of the strong winds. Additionally, all three dust storms occurred around noon local time during the summer. It is hypothesized that the temperature difference between the land and the atmosphere caused warm air to rise, prompting the surrounding air to flow toward the TD, generating strong winds and triggering dust storms.

Fig.5 shows the 2m temperature (°C), 850 hPa geopotential height (m), and 10 m horizontal wind ($m \cdot s^{-1}$) during the 8 dust storm events. Dust1-8 shows that the surface temperature in the Taklamakan Desert (TD) consistently exhibits high and evenly distributed temperatures. However, for Dust5, Dust7, and Dust8, the temperature in the TD region is notably higher than in other events. This increase in temperature can be attributed to the onset of May, which led to higher surface temperatures. Additionally, these three events occurred around noon, when solar radiation is strongest. The desert surface's higher specific heat capacity than the air resulted in a temperature difference between the surface and the atmosphere, creating an unstable atmospheric condition. This instability led to atmospheric convection, which generated strong winds and triggered dust storms.

In summary, the pressure gradient before dust storms in March and April is significantly greater than in May and June, while the surface temperature shows a marked increase from April to May. Therefore, dust storms occurring from March to June were categorized into two periods for analysis: spring (March and April) and summer (May and June).

3.3 Analysis of Dynamic and Thermodynamic Factors

https://doi.org/10.5194/egusphere-2025-4569
Preprint. Discussion started: 15 January 2026

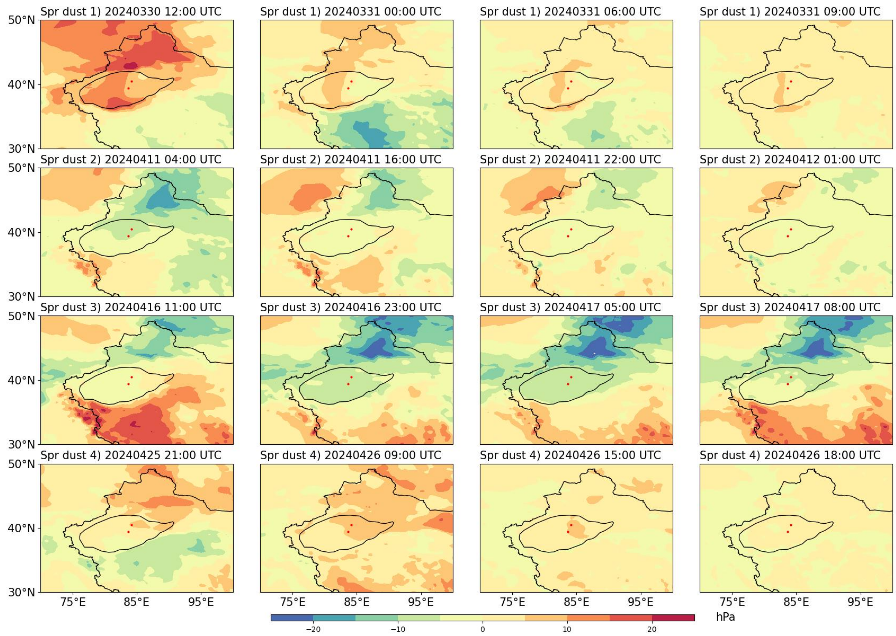

Fig.6 Spring sandstormΔ24h,Δ12h,Δ6h,Δ3h pressure difference

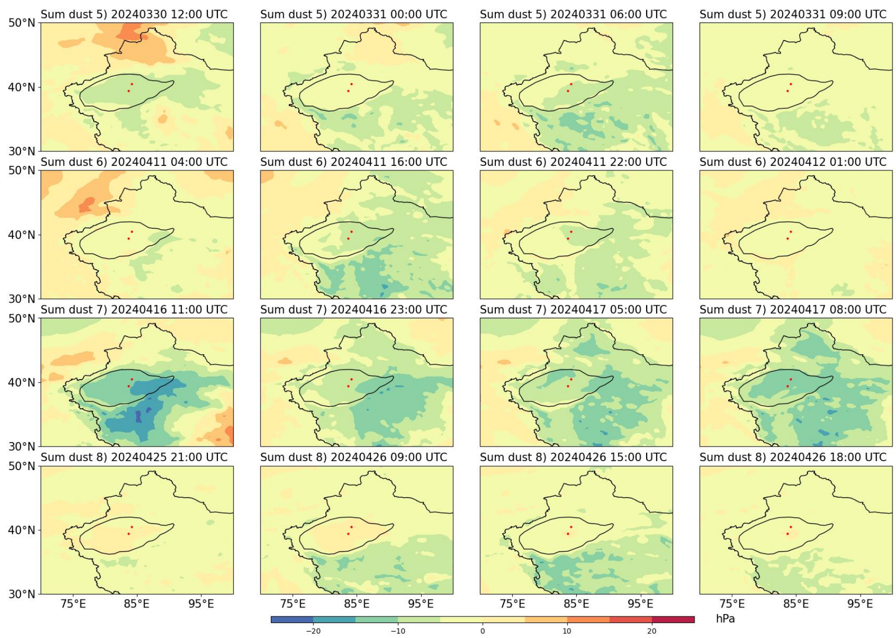

Fig.7 Summer sandstorm ΔP24h,ΔP12h,ΔP6h,ΔP3h pressure difference

Fig.6 and Fig.7 show the changes in average sea-level pressure over the 3, 6, 12, and 24 hours preceding the dust storms in the spring and summer periods, respectively. The calculation method involves subtracting the sea-level pressure at the specified times (3, 6, 12, and 24 hours before the dust storm) from the average sea-level pressure at the time of the dust storm. In the

https://doi.org/10.5194/egusphere-2025-4569
Preprint. Discussion started: 15 January 2026

figures, higher values indicate a greater increase in pressure, while lower values reflect a larger decrease in pressure.

In ΔP24h, during Dust1-7, the average sea-level pressure in the northern part of the Taklamakan Desert (TD) was lower than at the time of the dust storm. Additionally, for Dust2 and Dust3, the southwestern region also showed a lower pressure than that at the time of the storm. However, in ΔP12h, during Dust1-4, the pressure in the northern and southwestern parts of the Taklamakan Desert (TD) gradually increased but remained lower than the pressure at the time of the dust storm. In contrast, for Dust5-8, the pressure approached that at the time of the storm, and there were no significant changes in the subsequent ΔP6h and ΔP3h periods. For Dust1-4, there was little change in pressure from ΔP6h to ΔP3h, but it still differed significantly from the pressure at the time of the dust storm, especially for Dust3.

In summary, there is a clear difference in the pressure changes before dust storms in the spring and summer in the Taklamakan Desert (TD). In the spring, the pressure changes in the northern or southern parts of TD are significantly larger in ΔP24h compared to the summer, with a gradual increase in pressure in these areas leading up to the storm, forming a noticeable pressure gradient. This is consistent with the pressure difference observed during the dust storm. In the summer, the pressure at TD already approaches that at the time of the storm by ΔP12h, with little change afterward. Therefore, it can be inferred that pressure changes play a more direct and important role in the formation and development of dust storms in spring, while in summer, other factors may have a greater influence on dust storm occurrence.

Tab. 2 Variance and rangeΔP24h,ΔP12h,ΔP6h,ΔP3h before the dust storm

	Variance of ΔP24h	Range of variation	Variance of ΔP12h	Range of variation	Variance of ΔP6h	Range of variation	Variance of ΔP3h	Range of variation
dust1	49.91	(-10.66, 24.99)	35.37	(-17.82, 9.58)	11.55	(-11.37, 10.59)	3.76	(-5.75, 8.31)
dust2	34.9	(-19.23, 17.15)	28.06	(-14.77, 19.90)	16.01	(-14.64, 16.75)	7.27	(-15.91, 9.53)
dust3	71.14	(-17.23, 28.38)	59.21	(-25.17, 22.88)	67.81	(-25.47, 17.85)	83.14	(-24.15, 23.38)
dust4	26.18	(-14.89, 14.47)	12.95	(-6.59, 15.37)	4.24	(-4.99, 9.05)	1.24	(-2.84, 6.86)
dust5	19.22	(-10.14, 12.81)	10.29	(-12.25, 6.52)	11.73	(-16.05, 6.41)	3.36	(-8.55, 3.61)
dust6	11.47	(-8.78, 10.89)	19.8	(-16.58, 7.53)	8.25	(-11.44, 6.05)	2.66	(-6.79, 5.68)
dust7	45.82	(-21.66, 14.83)	21.26	(-16.02, 6.48)	21.45	(-17.80, 6.35)	23.27	(-19.91, 5.88)
dust8	2.82	(-7.51, 4.75)	10.48	(-13.80, 4.47)	11.32	(-17.07, 1.61)	3.26	(-9.90, 2.63)

Table 2 presents the variance and range of ΔP24h, ΔP12h, ΔP6h, and ΔP3h for the dust storms. Since the pressure difference effectively characterizes pressure changes, its variance reflects the intensity of pressure fluctuations. The analysis reveals that the range and variance in the spring (Dust1-4) are generally larger than in the summer (Dust5-8), indicating that pressure changes before dust storms in the spring are more intense. Notably, the pressure difference

https://doi.org/10.5194/egusphere-2025-4569
Preprint. Discussion started: 15 January 2026

between ΔP12h and ΔP6h for Dust1-4 shows significant variation, suggesting that the 12-hour to 6-hour period is when pressure fluctuations are most pronounced. Therefore, ΔP12h and ΔP6h could represent key windows for spring dust storm prediction. Closely monitoring pressure fluctuations during this phase can help predict the occurrence of dust storms in advance.

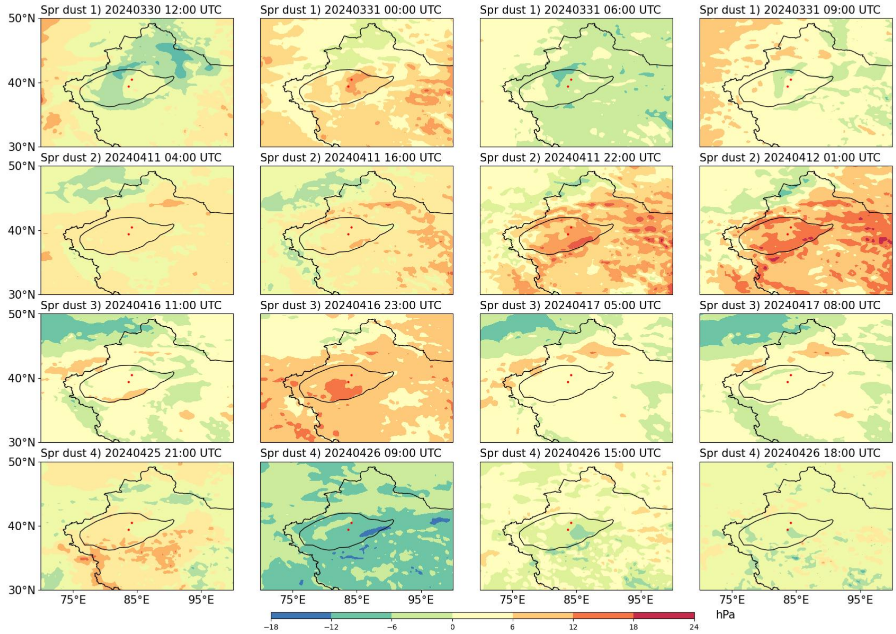

Fig.8 Spring sandstorm Δ 3, Δ 6, Δ 12, Δ 24 temperature difference

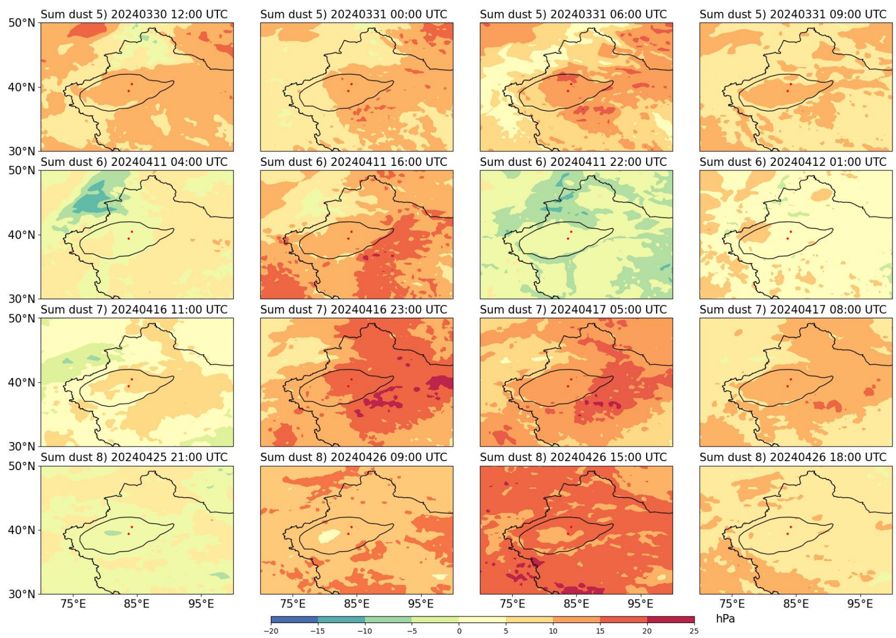

https://doi.org/10.5194/egusphere-2025-4569
Preprint. Discussion started: 15 January 2026

Fig.9 Summer sandstorm Δ 3, Δ 6, Δ 12, Δ 24 temperature difference

In desert regions or inland plateaus, the surface temperature increases dramatically, causing the near-surface air to expand and rise, leading to the formation of upward air currents. Upward air currents can trigger convection in specific areas or create strong winds that stir up surface dust, leading to dust storms. Figures 8 and 9 show the temperature changes 3, 6, 12, and 24 hours before the dust storms in spring and summer. Similar to the calculation of the average sea-level pressure, the larger the value, the lower the current temperature compared to the time of the dust storm, indicating more intense upward movement.

Both in spring and summer, the temperature changes in the Taklamakan Desert (TD) and surrounding areas are influenced by multiple factors, such as time of day and climate conditions, making the temperature variation complex. In spring, there is no clear trend in temperature changes, whereas in summer, most of the time is characterized by warming, particularly in the final three hours. In spring, only Dust2 shows a warming trend, whereas in summer, all processes exhibit a warming trend. Therefore, it can be inferred that temperature changes have a more significant impact on summer dust storms.

Tab. 3 Variance and range 24h, 12h, 6h, and 3h before the dust storm

		Variance of ΔP24h	Range of variation	Variance of ΔP12h	Range of variation	Variance of ΔP6h	Range of variation	Variance of ΔP3h
dust1	14.75	(-14.72, 11.67)	16.53	(-7.04, 20.38)	8.23	(-11.52, 6.52)	3.7	(-9.70, 2.56)
dust2	10.23	(-11.71, 8.58)	16.8	(-12.25, 14.16)	14.79	(-7.21, 17.02)	11.9	(-7.03, 15.44)
dust3	21.84	(-21.57, 4.40)	18.35	(-12.53, 16.39)	22.47	(-21.32, 8.41)	25.81	(-23.38, 8.48)
dust4	11.57	(-12.32, 11.02)	11.68	(-20.77, 0.23)	5.12	(-14.30, 3.57)	1.44	(-11.28, 5.12)
dust5	12.75	(-14.40, 8.30)	21.95	(-3.87, 22.52)	13.07	(-0.63, 20.23)	1.74	(-2.08, 8.17)
dust6	11	(-13.92, 6.40)	16.46	(-5.59, 20.28)	4.76	(-7.99, 7.40)	1.8	(-7.30, 4.06)
dust7	19.82	(-11.55, 16.01)	29.84	(-10.43, 22.44)	22.69	(-4.06, 27.81)	21.14	(-3.78, 25.95)
dust8	3.71	(-9.98, 6.68)	5.36	(-3.26, 14.72)	5.32	(-2.25, 15.46)	1.99	(-4.24, 8.42)

Table 3 shows the variance and range of temperature differences (ΔT) 24h, 12h, 6h, and 3h before the dust storm. Similar to the variance in pressure differences, the variance rapidly decreases between ΔT12h and ΔT6h, indicating a swift transition from a stable temperature state to an unstable state right before the dust storm occurs. This suggests that the ΔT12h-ΔT6h period is crucial for predicting summer dust storms.

3.4 Dust Flux Analysis

https://doi.org/10.5194/egusphere-2025-4569
Preprint. Discussion started: 15 January 2026

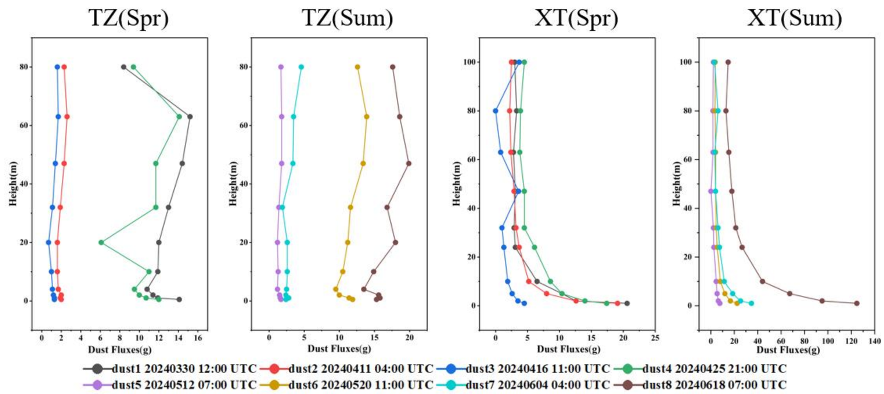

Fig.10 Schematic Diagram of Horizontal Dust Flux during Sandstorms (Left: TZ, Right: XT)

Fig.10 shows the horizontal dust flux (Q) at TZ and XT during spring and summer. The Q at TZ is mainly concentrated between 2g and 10-14g. When Q is low, the dust flux changes smoothly with height, showing no significant fluctuations. However, as Q increases, a noticeable upward trend appears between 47-63 cm, followed by a gradual decline, with a rapid increase in Q below 2m. According to Huo W (2022), the terrain at TZ is more undulating than XT and is influenced by natural dunes. As a result, the dust flux in this area shows an abnormal increase, highlighting the significant impact of topography on dust flux, especially in regions with strong winds or frequent dust activity. In such areas, topography plays a crucial role in dust transport.

The dust flux (Q) at XT exhibits a pattern similar to that of a parabolic function during spring and summer, gradually increasing as the height decreases. Q remains relatively stable between 100 and 24 meters, with slight fluctuation. However, once the height drops below 24 meters, the Q value rises significantly, especially in the near-surface layer (0 to 2 meters), where dust flux rapidly increases as the height decreases. This is due to the gravitational effect on dust particles, which tend to accumulate near the surface and are more easily lifted by the wind at lower altitudes.

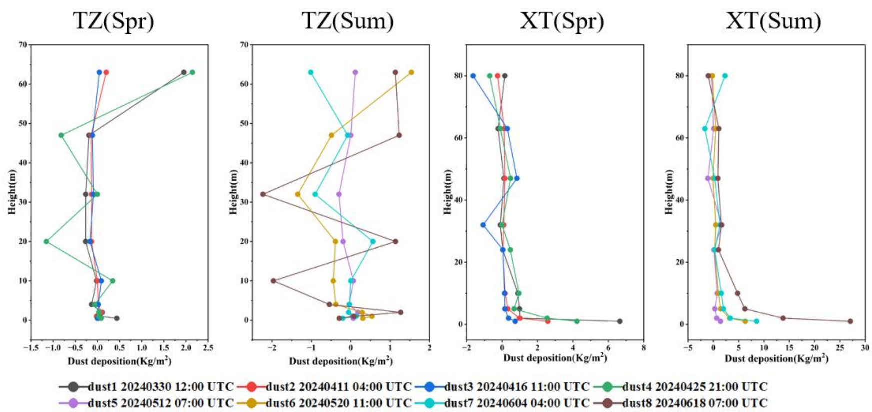

Fig.11 10 Schematic Diagram of Vertical Dust Flux during Sandstorms (Left: TZ, Right: XT)

Fig.11 illustrates the vertical dust flux (F) at TZ and XT during spring and summer. In

https://doi.org/10.5194/egusphere-2025-4569
Preprint. Discussion started: 15 January 2026

summer at TZ, the F values fluctuate more significantly. For example, in Dust 8, the F values oscillate between -2 and 1.5 kg/m², showing clear fluctuations. In contrast, the spring F values are more stable, with relatively minor changes; for Dust 1-3, the F values are mainly close to 0, indicating minimal vertical dust movement in the spring at TZ. On the other hand, during the summer, rapid surface temperature rise generates updrafts, causing more pronounced fluctuations in the F values. This suggests that temperature changes strongly influence dust storms at TZ in the summer.

The F curve at XT shows a similar trend to that of Q, exhibiting a pattern resembling a "bell-shaped curve," which suggests that the wind more easily lifts dust as height decreases. Additionally, the F values at XT show a similar trend in spring and summer, without the pronounced influence of temperature rise in TZ. This could be because TZ's more variable topography makes it more susceptible to temperature-induced updrafts. In contrast, XT's relatively flatter terrain may not experience such significant temperature effects, thus leading to more stable vertical dust flux behavior.

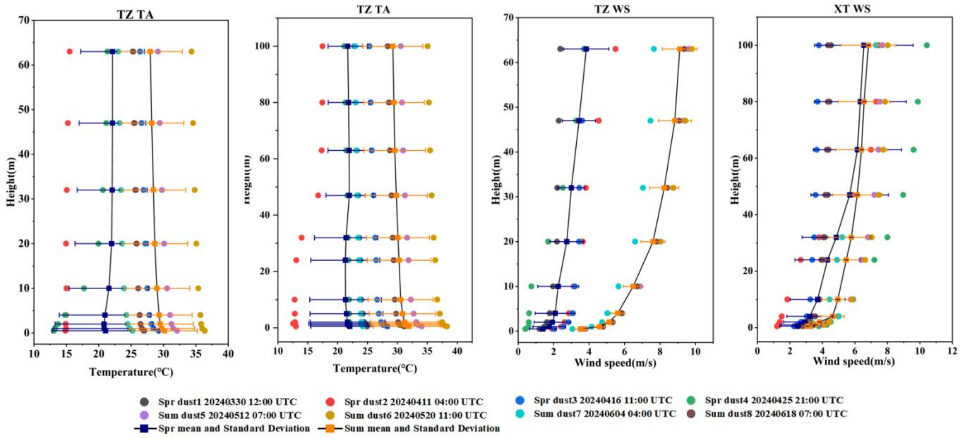

Fig.12 Schematic Diagram of Wind Speed and Temperature during Sandstorms (Left: TZ, Right: XT)

Fig.12 shows the temperature and wind speed variations during sandstorm events at the TZ and XT stations. The figure shows that the average temperature during summer sandstorms is 5-10°C higher than the normal summer temperature. Additionally, during summer sandstorms, the temperature at the lower levels of the stations is significantly higher than at higher levels. In contrast, lower temperatures are lower or comparable to those at higher levels during spring sandstorms.

At both TZ and XT, wind speed decreases with height. Comparing the wind speed variations between spring and summer, the amplitude of the wind speed change in spring is smaller than in summer. This phenomenon is likely related to the higher surface temperatures in summer, which increase the temperature difference between the surface and the atmosphere, making wind speed changes near the surface more intense. At TZ, the wind speed during summer sandstorms at higher levels is significantly higher than in spring, while the wind speed at lower levels is similar to that of spring. This is likely because spring sandstorms are dominated by horizontal winds, which are influenced by the undulating dunes, resulting in lower wind speeds at higher levels. In contrast, summer sandstorms are dominated by vertical winds and are less influenced by the terrain, thus showing a larger wind speed difference at higher levels. The terrain near the XT station is relatively flat, so the differences in wind speed variations between spring and summer are minor.

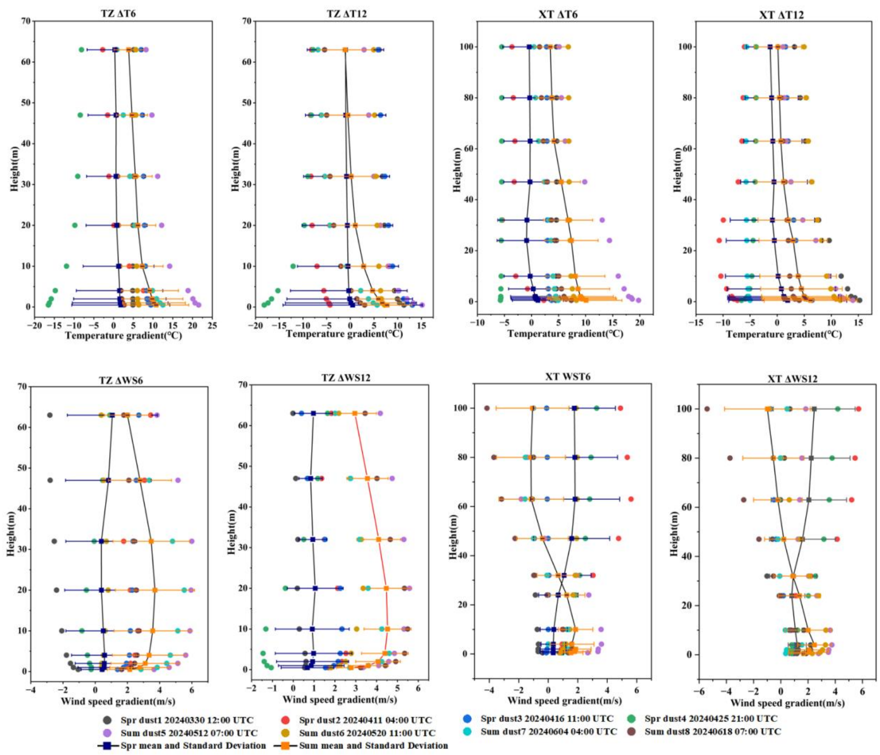

Fig.13 Schematic Diagram of Wind Speed and Temperature Changes (Δ6, Δ12) during Sandstorms (Left: TZ, Right: XT)

Figure 13 shows the temperature and wind speed changes 6 and 12 hours before the sandstorm event. It can be observed that, at both TZ and XT, the average ΔT6 and ΔT12 in summer are higher than those in spring, and the gap between them increases as the height decreases. This indicates that the temperature increase in summer is significantly higher near the surface than in spring, and as the height decreases, the temperature rise becomes more intense.

The wind speed variation chart for summer at XT shows a decrease in wind speed at higher levels, while wind speed at lower levels increases. In contrast, in spring, wind speed at higher levels increases, and wind speed at lower levels either remains unchanged or slightly increases. This phenomenon may be related to the fact that the XT station is located on the northern edge of TD, where the terrain is flat and not influenced by complex features such as dunes. The reasons for this will be discussed in the discussion section.

4 Discussion

4.1 Dust Trajectory Analysis

This study analyzes eight dust storm events in TD from March to June. Through trajectory analysis, it was found that the paths of dust storms entering the desert interior exhibit significant

https://doi.org/10.5194/egusphere-2025-4569
Preprint. Discussion started: 15 January 2026

diversity, but can be summarized into three main types.

The first type is the "East-Inflow" path, where most dust storms move from northeast to southwest. This path's formation is likely closely related to the topography surrounding TD: the northern and western parts of the desert are surrounded by high mountain ranges, while the eastern area has lower terrain, including the low-lying Lop Nur region. When a strong high-pressure system occurs in the northern regions, strong winds enter the desert through the lower terrain gaps, thus forming the East-Inflow path. The second type is the "Mountain-Crossing" path, where some strong winds enter the desert by crossing the western Tianshan Mountains or the Pamir Plateau. However, winds along this path are typically concentrated in the upper atmospheric layers, and their intensity is limited. The topographical barrier effect weakens the surface wind speed, with more of the driving force concentrated in the middle and upper levels of the atmosphere. The third type is the "Westward" path, primarily occurring during the two dust storms after June, with the trajectories moving from west to east. This path is likely related to the climatic characteristics of Central Asia. As summer arrives, the surface heating in the inland areas of Central Asia becomes more pronounced, leading to higher surface air temperatures around the desert. This temperature contrast affects the direction of air flow. When the dust storm approaches the desert, the larger surface-to-atmosphere temperature difference may cause a change in the direction of the airflow.

4.2 Discussion of Dynamic and Thermal Factors

This study further reveals the impact of dynamic and thermal mechanisms on dust storm processes. Analysis of the ERA5 data shows that from March to April, the TD region and its surroundings exhibit stronger pressure gradients, which favor the formation of strong winds. Additionally, within 24 hours before the dust storm event, spring sees significantly more dramatic pressure changes, aligning with the dynamic-dominated mechanism during this period. From May to June, the temperature at the desert surface rises significantly, increasing the temperature difference between the surface and the atmosphere. Furthermore, 24 hours before the dust storm, surface temperatures tend to increase in summer; in spring, temperatures either decrease or remain constant. This indicates that thermal factors dominate the formation of dust storms during the summer months.

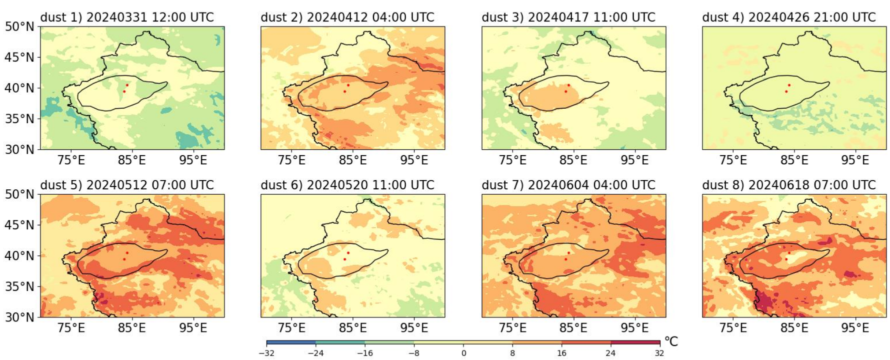

Fig.14 Temperature Difference in Dust Storms (Dust1-8)

To better explore the impact of temperature on dust storms, Figure 14 shows the surface-atmosphere temperature difference for Dust1-8. It can be observed that, except for Dust6, which occurred in the afternoon, the surface-atmosphere temperature difference in summer around TD and its surrounding areas is significantly higher than in spring. Additionally, from the periphery to the interior of TD, the temperature difference gradually decreases, indicating a transition from an unstable to a stable atmosphere, which suggests that dust is moving from the periphery of TD toward the desert interior.

Analysis of observational data reveals that in summer, both TZ and XT experience higher temperatures than in spring, with the temperature rise before dust storms being significantly greater in summer. Moreover, as height decreases, the temperature change becomes more intense. In contrast, the temperature difference in spring remains roughly around 0°C with height changes. This suggests that in the TD region, the overall temperature is higher in summer. However, the temperature increase is also significantly larger than in spring, especially in the lower altitude areas. Therefore, it can be inferred that spring temperature has a relatively minor impact on dust storms, while temperature in summer has a significantly larger effect.

For XT, the wind speed difference between spring and summer shows two distinctly different patterns. In summer, the wind speed at higher levels decreases, while at lower levels, it increases. In spring, the wind speed at higher levels increases, while the wind speed at lower levels remains constant or slightly increases. This could be due to the higher surface temperatures in summer, which increase the temperature difference and lead to intense convection, promoting updrafts and intensifying low-level wind speeds. At higher levels, the wind speed slightly decreases due to air sinking and a more stable atmosphere. In spring, with lower surface temperatures and smaller temperature differences, convection is weakened, and high-level wind speeds increase due to enhanced vertical stability. In contrast, low-level wind speeds remain relatively unchanged.

A comprehensive analysis from point to area was conducted by combining reanalysis data and observational data, further proving the seasonal differences in dust storm formation in the TD region. In spring, the primary driving force of dust storms is the pressure gradient, where the significant horizontal pressure difference leads to strong wind processes, triggering dust storms. In contrast, dust storms are mainly influenced by the difference in surface-atmosphere temperature in summer. The significant temperature contrast between the surface and the atmosphere creates intense instability, promoting enhanced convective activity and thereby intensifying the occurrence of dust storms. This multi-angle verification, from localized observations to regional reanalysis, further clarifies the dominant roles of dynamic and thermal factors in different seasons.

4.3 Key parameters are influenced by the terrain.

At the XT station (representing flat terrain), the dust flux (Q) exhibits a clear power-law function characteristic. In contrast, at the TZ station (representing undulating terrain), the dust flux (Q) shows a phased variation pattern. When Q values are high, an initial upward trend is followed by a decline, and then another increase. This variation may be attributed to secondary dust sources from the surrounding dunes, particularly influencing the mid-layer observational data, which causes an increase in dust flux within a specific altitude range. F exhibits a pattern similar to that of Q, but with more significant terrain differences. At the XT station, F remains relatively stable, whereas at the TZ station, F stabilizes around 0 kg/m² in spring. However, the variation increases in summer, oscillating between -2 and 1.5 kg/m². This phenomenon is likely due to the dominant influence of summer temperatures on vertical air currents.

5 Conclusion

The study is based on a dual-gradient observational experiment conducted in the central and peripheral regions of the Taklamakan Desert (TD), with eight observational samples obtained from April to June. Combined with ERA5 reanalysis data and the HYSPLIT backward trajectory model, the following conclusions were drawn:

The dust storm trajectories in the Taklamakan Desert (TD) can be classified into three types: first, dust storms travel from east to west, passing through the gaps in the Tianshan Mountains; second, they traverse the western Tianshan and the Pamir Plateau; and finally, after the onset of summer in June, the dust storm trajectories are dominated by thermal factors, initially moving from west to east, and then shifting from the northeast to the southwest into the desert.

Dynamic factors primarily drive dust storms in the TD in March and April, where strong winds caused by pressure gradients lead to dust storms. In May and June, thermal factors dominate, with temperature differences between the surface and the atmosphere triggering convection that results in dust storms. Additionally, the period 12 to 6 hours before the dust storm is characterized by significant changes in atmospheric pressure and temperature, which can be used as a key time window for predicting the occurrence of dust storms.

At the XT station, representing flat terrain, Q and F rapidly increase near the surface, following a power-law function pattern. At the TZ station, representing undulating terrain, Q shows a similar power-law function-like curve when values are high. However, fluctuations in mid-level Q are caused by secondary dust sources from dunes. On the other hand, F is influenced by both terrain and thermal factors, with minor fluctuations in spring and larger fluctuations in summer. During summer, both stations experience significantly higher temperatures and more pronounced temperature changes compared to spring, highlighting the more decisive influence of summer temperatures on dust storms. Additionally, the variability in wind speed at the XT station during summer indicates that wind speed changes are primarily influenced by seasonal temperature differences, convective intensity, and the flat terrain of the area.

Acknowledgements

We gratefully acknowledge the National Earth System Science Data Center (http://www.geodata.cn) and the Institute of Desert Meteorology (China Meteorological Administration, Urumqi) for providing essential datasets. We also extend our thanks to the College of Geography and Remote Sensing Science, Xinjiang University (Urumqi), for their technical support.

Author Contributions

Y.W. : Conceptualization , Writing – original draft , Formal Analysis.

WH.:Methodology, Supervision, Writing - review. & editing.

YL.:Validation.

M.M : Investigation, Data Curation.

F.Y: Experimental Design, Supervision.

C.Z..X.Y.A.M.: Investigation , Data Curation.

Funding

This work was supported by the Tianshan Talent Project of Xinjiang (Grant No. 2023TSYCCX0075), the China Meteorological Administration Youth Innovation Team Project (Grant No. CMA2024QN13), the National Natural Science Foundation of China (42207134), and the Xinjiang Science and Technology Innovation Team (Tianshan Innovation Team) Project (Grant No. 2022TSYCTD0007).

Data availability

The meteorological observational data used in this study are maintained and owned by the Institute of Desert Meteorology, China Meteorological Administration, located in Urumqi, Xinjiang, China, and are subject to institutional regulations and access restrictions. ERA5 reanalysis datasets were obtained from the European Centre for Medium-Range Weather Forecasts (ECMWF) through the Copernicus Climate Data Store (https://cds.climate.copernicus.eu). Researchers or interested parties who wish to obtain access to the observational datasets may submit a formal request to the Institute of Desert Meteorology, outlining the purpose and scope of their intended use. Approval of such requests will be at the discretion of the institute, in accordance with its data-sharing policies.

Competing Interests

The authors declare no competing interests.

References

Achakulwisut, P., Mickley, L. J., & Anenberg, S. C. (2018). Drought-sensitivity of fine dust in the US Southwest: Implications for air quality and public health under future climate change. *Environmental Research Letters*, *13*(5), 054025. https://doi.org/10.1088/1748-9326/aabf20

Aili, A., Xu, H., Xu, Q., & Liu, K. (2023). Aeolian dust movement and deposition under local atmospheric circulation in a desert-oasis transition zone of the northeastern Taklimakan desert. *Ecological Indicators*, *157*, 111289. https://doi.org/10.1016/j.ecolind.2023.111289

Bao, C., & Fang, C. (2007). Water resources constraint force on urbanization in water deficient regions: A case study of the Hexi Corridor, arid area of NW China. *Ecological Economics*, *62*(3–4), 508–517. https://doi.org/10.1016/j.ecolecon.2006.07.013

Chen, S., Zhao, D., Huang, J., He, J., Chen, Y., Chen, J., Bi, H., Lou, G., Du, S., Zhang, Y., & Yang, F. (2023a). Mongolia Contributed More than 42% of the Dust Concentrations in Northern China in March and April 2023. *Advances in Atmospheric*

Sciences, *40*(9), 1549–1557. https://doi.org/10.1007/s00376-023-3062-1

Chen, S., Zhao, D., Huang, J., He, J., Chen, Y., Chen, J., Bi, H., Lou, G., Du, S., Zhang, Y., & Yang, F. (2023b). Mongolia Contributed More than 42% of the Dust Concentrations in Northern China in March and April 2023. *Advances in Atmospheric Sciences*, *40*(9), 1549–1557. https://doi.org/10.1007/s00376-023-3062-1

Chen, Y., An, J., Qu, Y., Xie, F., & Ma, S. (2023). Dust radiation effect on the weather and dust transport over the Taklimakan Desert, China. *Atmospheric Research*, *284*, 106600. https://doi.org/10.1016/j.atmosres.2022.106600

DeMeester, T. R., & Johnson, L. F. (1975). Evaluation of the Nissen antireflux procedure by esophageal manometry and twenty-four hour pH monitoring. *American Journal of Surgery*, *129*(1), 94–100. https://doi.org/10.1016/0002-9610(75)90174-9

Gillette, D. A., & Passi, R. (1988). Modeling dust emission caused by wind erosion. *Journal of Geophysical Research: Atmospheres*, *93*(D11), 14233–14242. https://doi.org/10.1029/JD093iD11p14233

Hosseini Dehshiri, S. S., & Firoozabadi, B. (2024). Dust emission, transport, and deposition in central Iran and their radiative forcing effects: A numerical simulation. *Atmospheric Pollution Research*, *15*(11), 102267. https://doi.org/10.1016/j.apr.2024.102267

Huo, W., Song, M., Wu, Y., Zhi, X., Yang, F., Ma, M., Zhou, C., Yang, X., Mamtimin, A., & He, Q. (2022). Relationships between Near-Surface Horizontal Dust Fluxes and Dust Depositions at the Centre and Edge of the Taklamakan Desert. *Land*, *11*(7), 959. https://doi.org/10.3390/land11070959

Iversen, J. D., & White, B. R. (1982). Saltation threshold on Earth, Mars and Venus. *Sedimentology*, *29*(1), 111–119. https://doi.org/10.1111/j.1365-3091.1982.tb01713.x

Kai, Z., & Huiwang, G. (2007). The characteristics of Asian-dust storms during 2000–2002: From the source to the sea. *Atmospheric Environment*, *41*(39), 9136–9145. https://doi.org/10.1016/j.atmosenv.2007.08.007

Liu, J.-T., Jiang, X.-G., Zheng, X.-J., Kang, L., & Qi, F.-Y. (2004). An Intensive Mongolian Cyclone Genesis Induced Severe Dust Storm. *Terrestrial, Atmospheric and Oceanic Sciences*, *15*(5), 1019. https://doi.org/10.3319/TAO.2004.15.5.1019(ADSE)

Ma, M., Yang, X., He, Q., Zhou, C., Mamtimin, A., Huo, W., & Yang, F. (2020). Characteristics of dust devil and its dust emission in northern margin of the Taklimakan Desert. *Aeolian Research*, *44*, 100579. https://doi.org/10.1016/j.aeolia.2020.100579

MacKinnon, D. J., Clow, G. D., Tigges, R. K., Reynolds, R. L., & Chavez, P. S. (2004). Comparison of aerodynamically and model-derived roughness lengths (zo) over diverse surfaces, central Mojave Desert, California, USA. *Geomorphology*, *63*(1–2), 103–113. https://doi.org/10.1016/j.geomorph.2004.03.009

Manisalidis, I., Stavropoulou, E., Stavropoulos, A., & Bezirtzoglou, E. (2020). Environmental and Health Impacts of Air Pollution: A Review. *Frontiers in Public Health*, *8*, 14. https://doi.org/10.3389/fpubh.2020.00014

Marticorena, B., & Bergametti, G. (1995). Modeling the atmospheric dust cycle: 1. Design of a soil-derived dust emission scheme. *Journal of Geophysical Research:*

https://doi.org/10.5194/egusphere-2025-4569
Preprint. Discussion started: 15 January 2026

Atmospheres, *100*(D8), 16415–16430. https://doi.org/10.1029/95JD00690

Mohebbi, A., Green, G. T., Akbariyeh, S., Yu, F., Russo, B. J., & Smaglik, E. J. (2019). Development of Dust Storm Modeling for Use in Freeway Safety and Operations Management: An Arizona Case Study. *Transportation Research Record: Journal of the Transportation Research Board*, *2673*(5), 175–187. https://doi.org/10.1177/0361198119839978

Perez, L., Tobias, A., Querol, X., Künzli, N., Pey, J., Alastuey, A., Viana, M., Valero, N., González-Cabré, M., & Sunyer, J. (2008). Coarse Particles From Saharan Dust and Daily Mortality. *Epidemiology*, *19*(6), 800–807. https://doi.org/10.1097/EDE.0b013e31818131cf

Prospero, J. M. (1999). Long-range transport of mineral dust in the global atmosphere: Impact of African dust on the environment of the southeastern United States. *Proceedings of the National Academy of Sciences*, *96*(7), 3396–3403. https://doi.org/10.1073/pnas.96.7.3396

Raupach, M. R. (1992). Drag and drag partition on rough surfaces. *Boundary-Layer Meteorology*, *60*(4), 375–395. https://doi.org/10.1007/BF00155203

Rizza, U., Barnaba, F., Miglietta, M. M., Mangia, C., Di Liberto, L., Dionisi, D., Costabile, F., Grasso, F., & Gobbi, G. P. (2017). WRF-Chem model simulations of a dust outbreak over the central Mediterranean and comparison with multi-sensor desert dust observations. *Atmospheric Chemistry and Physics*, *17*(1), 93–115. https://doi.org/10.5194/acp-17-93-2017

Shao, Y., & Dong, C. H. (2006). A review on East Asian dust storm climate, modelling and monitoring. *Global and Planetary Change*, *52*(1–4), 1–22. https://doi.org/10.1016/j.gloplacha.2006.02.011

Stein, A. F., Draxler, R. R., Rolph, G. D., Stunder, B. J. B., Cohen, M. D., & Ngan, F. (2015). NOAA's HYSPLIT Atmospheric Transport and Dispersion Modeling System. *Bulletin of the American Meteorological Society*, *96*(12), 2059–2077. https://doi.org/10.1175/BAMS-D-14-00110.1

Sun, J., & Liu, T. (2006). The Age of the Taklimakan Desert. *Science*, *312*(5780), 1621–1621. https://doi.org/10.1126/science.1124616

Tong, D., Feng, I., Gill, T. E., Schepanski, K., & Wang, J. (2023). How Many People Were Killed by Windblown Dust Events in the United States? *Bulletin of the American Meteorological Society*, *104*(5), E1067–E1084. https://doi.org/10.1175/BAMS-D-22-0186.1

Wang, H., Jia, X., Li, K., & Li, Y. (2015). Horizontal wind erosion flux and potential dust emission in arid and semiarid regions of China: A major source area for East Asia dust storms. *CATENA*, *133*, 373–384. https://doi.org/10.1016/j.catena.2015.06.011

Wang, X., Zhai, P., & Wang, C. (2009). Variations in extratropical cyclone activity in northern East Asia. *Advances in Atmospheric Sciences*, *26*(3), 471–479. https://doi.org/10.1007/s00376-009-0471-8

Wang, Y., Gao, J., Mamtimin, A., Sayit, H., Zhou, C., Li, R., Dawut, M., Yang, F., Huo, W., Wen, C., Song, M., & Aihaiti, A. (2023). Evolution law of atmospheric boundary layer in Gurbantünggüt Desert based on reanalysis dataset and in situ observation data. *Heliyon*, *9*(3), e14147.

https://doi.org/10.5194/egusphere-2025-4569
Preprint. Discussion started: 15 January 2026

https://doi.org/10.1016/j.heliyon.2023.e14147

Wen, H.-J., Wang, S.-L., Wu, C.-D., & Liang, M.-C. (2024). Association of Asian dust storms and PM2.5 with clinical visits for respiratory diseases in children. *Atmospheric Environment*, *333*, 120631. https://doi.org/10.1016/j.atmosenv.2024.120631

Xu, C., Guan, Q., Lin, J., Luo, H., Yang, L., Tan, Z., Wang, Q., Wang, N., & Tian, J. (2020). Spatiotemporal variations and driving factors of dust storm events in northern China based on high-temporal-resolution analysis of meteorological data (1960–2007). *Environmental Pollution*, *260*, 114084. https://doi.org/10.1016/j.envpol.2020.114084

Yang, X., Shen, S., Yang, F., He, Q., Ali, M., Huo, W., & Liu, X. (2016). Spatial and temporal variations of blowing dust events in the Taklimakan Desert. *Theoretical and Applied Climatology*, *125*(3–4), 669–677. https://doi.org/10.1007/s00704-015-1537-4

Zeng, X., & Dickinson, R. E. (1998). Effect of Surface Sublayer on Surface Skin Temperature and Fluxes. *Journal of Climate*, *11*(4), 537–550. https://doi.org/10.1175/1520-0442(1998)011<0537:EOSSOS>2.0.CO;2

Zeng, Y., Wang, M., Zhao, C., Chen, S., Liu, Z., Huang, X., & Gao, Y. (2020). WRF-Chem v3.9 simulations of the East Asian dust storm in May 2017: Modeling sensitivities to dust emission and dry deposition schemes. *Geoscientific Model Development*, *13*(4), 2125–2147. https://doi.org/10.5194/gmd-13-2125-2020

Zhang, H., Cisse, M., Dauphin, Y. N., & Lopez-Paz, D. (2017). *mixup: Beyond Empirical Risk Minimization* (Version 2). arXiv. https://doi.org/10.48550/ARXIV.1710.09412

Zong, Q., Mao, R., Gong, D.-Y., Wu, C., Pu, B., Feng, X., & Sun, Y. (2021). Changes in Dust Activity in Spring over East Asia under a Global Warming Scenario. *Asia-Pacific Journal of Atmospheric Sciences*, *57*(4), 839–850. https://doi.org/10.1007/s13143-021-00224-7